Chapter 1

Introduction

1.1. General introduction

This study is primarily focused on the understanding of geological systems by the aid of computers, the "intelligence amplifiers" (see Merriam, 2004). Three geological problems are discussed in the forthcoming chapters, focused on economic, structural and sedimentary geology related themes:

- Exploration for Pb-Zn mineral deposits of large tonnage (Lawn Hill Region),
- Understanding the genesis of the Century zinc deposit,
- Reconstruction of the processes that led to the formation of the Middle Cambrian Lawn Hill Megabreccia.

A primary objective is to obtain temporal and spatial reconstructions of the geological evolution of each component, or sub-system of the study area, the Lawn Hill Region in northern Queensland, Australia. The project was specifically aimed at using advanced computational tools to analyse geological variables, but it also involved the development of computer software to solve specific problems.

1.2. Application of computer science to geology

I have been always fascinated by computers therefore as a geologist I decided that I wanted to prove to myself that the computer "is worth a try in geology". When I started this project I had already gained experience with the use of computers in geology mainly developing geological models in 3D and producing animations of geological terrains, taking the audience across dynamic, virtual scenarios to observe structural characters with great detail. Most importantly the virtual experience was a way to deliver quickly the information to them at different scales (zooming up and down). This first attempt was driven by the understanding that computers extend our ability to represent multivariate systems. In the end it revealed also that frequently these methodologies are so fascinating that the science behind these models becomes of secondary importance for the unaware audience. This should not happen. Science has long been fascinating for its simplicity not for its technicality.

Stepping from the "glossy animations" I approached the real potential of such tools in addressing a classic topic of Economic Geology – ore genesis. Computer software such as GoCAD, FLAC, FLAC-3D and some programs I developed were used to reconstruct several mineral deposit scenarios. The results were integrated to offer a vision of ore genesis obtained from the different modelling perspectives.

The interrelationship among humans and machines is now so deep that it is becoming difficult to evaluate if the benefit is derived exclusively from the machine itself (hardware) (e.g. Merriam, 1999) or from the software developed by hundreds of developers. In other words computers are now not only huge databases, they also have

the ability to store and retrieve our intellect (correlating data and developing inferences) in the form of high level computer software (structured languages). This process is iterative, irreversible and gradually sees the transfer and upgrade of knowledge from humans to machines (e.g. the OpenSyc, Formalized Common Knowledge project; http://www.opencyc.org), until perhaps the computers will start to think autonomously. These perspectives were, in part, the reason for a second stage of the project devoted to the exploration of mineral deposits in the Lawn Hill Region using empirical modelling of probability. In this context the application of computers to geology assumes a role that is different from the previous, because computer programs are not exclusively a representation of a multivariate system and how its variables are related to one another. Boolean logic takes the place of partial differential equations (used in process modelling) to empirically explore interlocked variables in this case, but the main difference is that the computer software provides a final output that is derived from an automated inference mechanism- the Bayesian reasoning.

A geological problem can be addressed quantitatively in different manners; the same dataset can be fitted using several mathematical models (Krumbein, 1962). This raises the question of what technique is the best and which one should be used. However, there is no clear answer to this. More likely it is better to favour the fusion (integration involving rejection of poor models) of diverse mathematical models rather than limit the analysis (i.e. the search for mineral deposits as function of a single ore genetic model). The problem is how to define the goodness of fit of our models (e.g.

Fisher, 1925). This leads to a final stage in this thesis - the relationship of qualitative versus quantitative geology.

Computational modelling is certainly an improved methodology, which deals more adequately with geological complexity. Therefore it represents a valid alternative to more consolidated (conventional) methodologies of analysis, of geological problems. For example (see Chapter 3), modern digital mapping tools have effectively been valuable alternatives to conventional outcrop mapping, when exploring for mineral deposits. Nonetheless, the quality of field based studies retain its importance for obvious reasons. Similarly, when treating quantitatively and computationally the problem of genesis and timing of a geological event (Chapters 4-6) a multi-dimensional (space, time) perspective is available. Multi-dimensionality leads to better conceptualisation of a geological system. With computational modelling a more comprehensive vision is offered to the geologists, which are then able to test their hypothesis more elegantly. Quantitative modelling is therefore a natural step (required) to improve the qualitative methodology of the past, but it should never be considered as a way to avoid *a priori* qualitative assessment.

1.3. Aims and objectives

In summary this study had the following aims:

- Compile software that allows constructing predictive exploration GIS models that make use of Bayesian probability analysis, (Chapter 3);

- construct and run 3D models and simulations to understand the genesis of the Century zinc deposit, (Chapters 4 and 5);
- combine qualitative and quantitative analysis to understand the timing and origin of the Lawn Hill Megabreccia, (Chapter 6); and
- synthesis and conclusions (Chapter 7).

In addition to the application of commercial softwares in all chapters, additional computer code was developed in Visual Basic to address both small and large scale issues or to extend the functionalities of proprietary software such as GoCAD (see Appendix C).

1.4. Thesis outline

Chapter 1 Introduction

The first chapter is a general introduction to the thesis work, discussing how the work explores different types of computer applications to geology.

Chapter 2 Historic overview and modelling background

The second chapter discusses the historical background that has in part guided the author toward this study. Firstly the evolution of numerical geological science is examined, becoming progressively quantitative although the qualitative, observational side remains still rooted and essential. This mathematisation process is complemented by the introduction of computers and programs designed to solve geological problems.

The chapter then concludes with a general overview and theoretical background of the type of applications used in chapters 3-6.

Chapter 3 An integrated knowledge-based and data-driven modelling study of the Lawn Hill Region, Queensland, Australia

This chapter compares, at regional scale, a knowledge-driven model based on expert driven scores using common knowledge of SEDEX-type deposits and MVT-type deposits, and a data-driven model developed using Bayesian analysis with the Weights of Evidence method. Considerations are made concerning the validity of the two methodologies and of the benefit derived from their integration.

Chapter 4 Testing the structural and geomechanical processes in the formation of the Century Zn-Pb-Ag Deposit

The fourth chapter is a camp-scale to deposit-scale study focused on the Century deposit aiming at understanding and testing different ore genetic models for the Zn-Pb-Ag mineralisation. Camp-scale reconstructions focus on the understanding of the structural evolution and role of faulting in contributing to the spatial distribution of mineral grades. Numerical 2D simulations of deformation and fluid flow are also presented to test previously proposed genetic models.

Chapter 5 Modelling the giant, Zn-Pb-Ag Century deposit, Queensland, Australia

The fifth chapter is a deposit scale study. The interrelationship between faulting and mineralisation and the role of other controlling variables is evaluated, to understand the spatial patterning of mineralisation. Inferences derived from the integration of 3D structural and property modelling combined with 3D coupled fluid flow and deformation numerical simulations are considered in the context of basin history, emphasising the importance of basin compartmentalisation.

Chapter 6 Catastrophic mass failure of a Middle Cambrian platform margin, the Lawn Hill Megabreccia, Queensland, Australia

The sixth chapter is a deposit scale study of the Middle Cambrian limestones unconformably covering Century. The study represents an example of how quantitative geology can be combined with observational qualitative, field based studies to resolve complex geological scenarios (i.e. multiple phases of breccia development).

Chapter 7 Complexity and self-organisation

The seventh chapter proposes an alternative non-linear view of geological processes suggesting that complex patterning (e.g. mineral deposit formation, breccia development etc.) and randomness can be treated with an innovative approach that combines deterministic with probabilistic laws.

Chapter 8 Conclusions

This final chapter contains a brief summary of the conclusions, and a general conclusive statement.

Appendix A-B

Mathematical models (technical background).

Appendix C

Software developed.

Appendix D

Table of specimens used in the thesis.

Appendix E

- Digital copy of the thesis.
- PowerPoint animation of 3D structural and property model of the Century deposit.
- WofE-2D software.
- High resolution Figs 3.1 and 5.7

Chapter 2

Historic overview and modelling background

Acknowledgement of Contributions

N.H.S. Oliver – normal supervisory contributions

2.1 Introduction

This chapter considers a historic overview that focuses on the gradual shift from qualitative to quantitative geology looking also at the advances that the use of computer has brought into quantitative geology. Retracing this history underlies important connections of present applications with the past. These references clarify the derivation of the approaches adopted in the thesis and the theoretical paths used to explore the geological problems. The chapter concludes with a section that provides the theoretical background relative to the statistical and deterministic models applied later in this thesis.

The work treated in the core of the thesis considers "decision functions" in a mineral exploration case. 3D models are also constructed using interpolation algorithms derived from geostatistical methods (e.g. Mallet, 1989). These quantitative approaches are statistical and use software tools derived from advances in mathematical geology (Howarth, 2001). In addition to this, deterministic simulations (e.g. fluid flow and deformation in sedimentary basins, Bethke et al., 1988) were also generated with the aid of fast workstations to study the physical processes that involve migration of fluids in and around faults in sedimentary basins.

The historical perspective draws marked lines between these models. This division derives from the philosophical approach adopted to solve scientific problems that see two distinct methodologies: the *deterministic* based on sets of equations that fully

describe the system with a finite number of variables, and the *statistical* approach based on stochastic models with equations that fit a real system with infinite variables. In this regard Agterberg (1967) discusses some of the methodologies adopted to better understand stochastic processes, illustrating the evolution from Surface Trend Analysis to other more refined methods of regression including *geostatistical approaches* (e.g. moving average), *Poisson distribution*, the use of *Fourier-transform* and *Power Spectra analysis*. The counterpart to such statistical models is matched by the sophistication of *finite-difference* techniques in numerical simulations (e.g. Harbaugh and Bonham-Carter, 1970).

2.2 Historic overview

2.2.1 From qualitative to quantitative geology

The roots of quantitative geology are very deep (Merriam, 1981; Howarth, 2001; Merriam, 2004). For instance, Agricola made use of trigonometry in mining applications as he reports on his book the De Re Metallica (Merriam, 2004). However, even earlier is the estimation of the earth circumference based on astronomical observations of the sun by Eratosthenes (276-194 BC) in ancient Greece (Fig. 2.1).

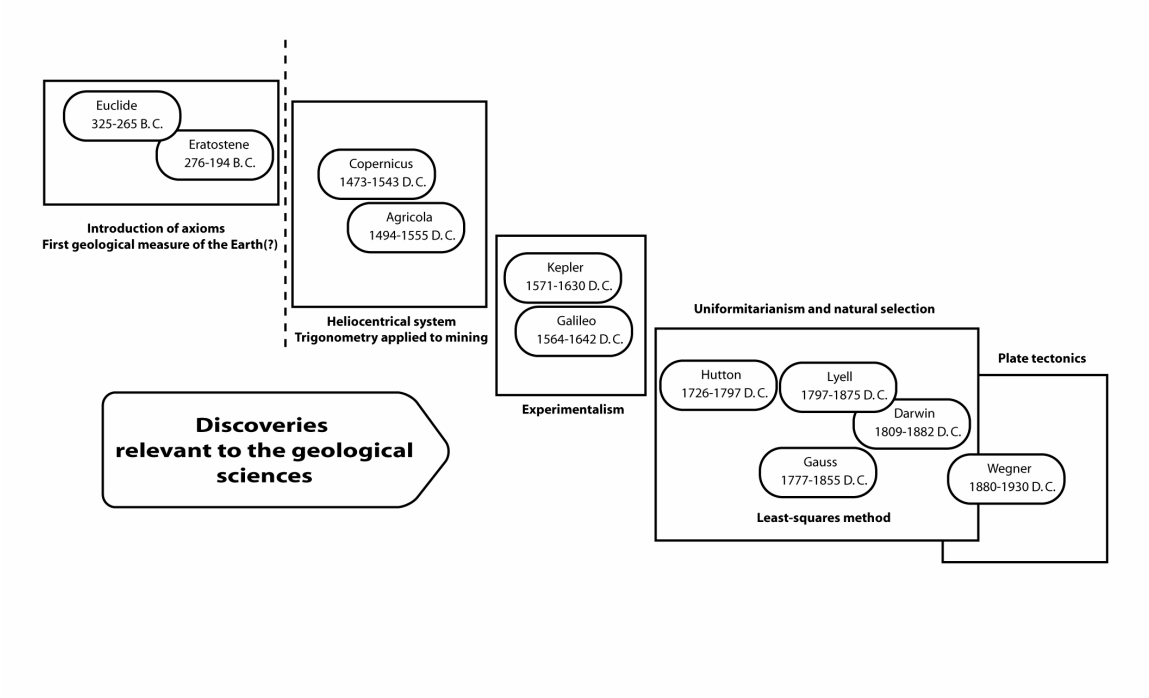

Fig. 2.1 Diagram showing a summary of the personalities that influenced the history of science and as a consequence contributed directly and indirectly to the advance in natural sciences including geology.

Unfortunately in the past, practitioners of quantitative methods were few, and the application of mathematical and statistical methods to geology required several scientific revolutions to gain consideration, including the advent of computers. At the beginning of the 17th Century, only after Galileo and Kepler "the experimentalists" (see Einstein, 1934), a quantitative approach to science became a necessary requirement to improve theoretical models. However, a considerable time after this philosophical advance was still necessary for a young discipline such as geology to become effectively numerated.

Early theories such as plutonism (Hutton, 1726-1797), uniformitarianism (Lyell, 1797-1875), and plate tectonics (Wegner, 1880-1930) were mostly the success of an observational science. Wegner, in fact, proposed his theory initially by noting a similarity among the margins of continents. Qualitative reasoning was therefore a primary tool that also became more refined later after Chamberlain introduced the method of "multiple working hypothesis" in 1897 (Krumbein, 1962). A qualitative approach could certainly grasp generalised laws of nature such as natural selection (Darwin 1809-1882). However, early scientific investigations have been turned to more rational and careful analysis of experience, leading to the present reductionism. Reductionism can be exemplified by modern experiments in particle physics. Understanding simple parts of a system at sub-atomic scale (non-observable) requires inevitably a quantitative approach. Qualitative holist science must therefore become reductionist quantitative science, reflecting the need of extending our scientific experiences. Reductionism remains also unavoidable as it is far easier to describe independently the element of a system rather than look at the whole, because this would require a full understanding of variable interactions (the variable interlocking of Krumbein) a task that is often impossible to fully achieve, hence the use of statistical methods. There seems to be then, a natural tendency towards quantitative geology as shown by Merriam (2004) in the exponential trend and relative stages of evolution of mathematical sciences (Fig. 2.2). The application of mathematics and

computer science to geology can also be understood by looking at the history of the scientists that contributed to them (Fig. 2.3).

Fig. 2.2 Diagram illustrating the different stages of development of quantitative geology. Modified from Merriam (2004). An additional stage is considered that forecasts the advent of intelligent systems.

Fig.2.3 Tree of quantification portraying some names of eminent researchers involved with the interrelationships of physical and natural sciences. Some of these figures contributed to the mathematisation of the geological science. Adapted from Merriam (2004).

2.2.2 Regression

Howarth (2001) provides an excellent description of how regression and model-fitting methods have evolved in earth sciences. This section adapts then the historic reconstruction of Howarth showing the derivation of statistical and deterministic methods.

Howarth (2001) reports a historical study of magnetic declination, which probably was the first example of application of quadratic functions to predict the variation of the earth's magnetic field. This work was developed by a mathematical practitioner, Henry Bond (1600-1678), who predicted correctly the magnetic declination in London for the year 1657 and subsequently published a series of manuscripts with 30 years forecasts of magnetic declination. Other historical studies were more focused on astronomical observations and the measuring of the Earth's shape, which led to the development of new mathematical formulations, respectively developed by Mayer (1723-1762) and Boskovic (1711-1787), but also others (Howarth, 2001). However, only at the end of the 18th Century did the German mathematician Gauss (1777-1855) develop a new method to fit a generic mathematical equation to a finite number of data points. This was the famous least square method that he firstly applied to interpolate the elliptical orbit of an inferred planet (the planetoid Ceres). The least-squares method is mathematically expressed as the minimization of the sum of the squared residuals (e_i) that is the difference between

measured (y_i) and computed ($\hat{y}_i$) values derived from the mathematical model fitted to the data, where *n* refers to the number of measured values:

$$\sum_{i=n} e_i^2 = \sum_{i=n} \left(y_i - \hat{y}_i \right)^2 \mapsto 0 \qquad (2.1).$$

The first publication of the method is attributed to Legendre (1752-1833) in 1805 who published the method as a way to determine cometary orbits. From this stage, the least-squares method was progressively divulged by Gauss (e.g. models of the global magnetic field, see Fig. 2.4) and others (e.g. Airy, 1801-1892).

However, significant progress in regression analysis as it is known to modern scientists (e.g. Sahoo and Pandalai, 1999), had to wait until the beginning of the 20th century when the work of Pearson (1857-1936) and his collaborator Yule (1871-1951) elucidated the connection existing between least-squares and the regression line coefficients (β_0, β_1), which could be represented as the intersection of a line with the ordinate axis and angular coefficient of a linear function in *y* (*x*) of type:

$$y_i = \beta_o + \beta_1 x_i \qquad (2.2).$$

Equations (1) and (2) can be combined to derive the best coefficients for $y(x)$ that fit randomly collected data of a population:

$$\sum_{i=n} e_i^2 = \sum_{i=n} \left(y_i - \left(\beta_o + \beta_1 x_i \right) \right)^2 \mapsto 0 \qquad (2.3).$$

The least-squares method being coupled with the regression line became effectively a statistical tool for bi- and multivariate analysis. However, it was only after Fisher (1890-1962) that a firm theoretical basis was set in a definitive manner. Fisher (1925) introduced concepts such as the variance of a population (the residuals gained importance rather than being neglected) and formal tests for statistical significance of coefficients (β_0, β_1) in the regression equation (Howarth, 2001). In the second quarter of the 20th Century the efforts of Krumbein (1902-1979) (one of the fathers of mathematical geology) led to widespread application of mathematics and statistics to sedimentary geology problems, e.g. Manual of Sedimentary Petrography (Krumbein and Pettijohn, 1938). Krumbein was interested in discriminating between large trends in sedimentary facies distributions and local anomalies. His contribution led to the extension of the least-squares fitting method to the approximation of polynomial functions representing regional datasets that were approximated either by linear or non-linear surfaces. This

method was named Trend-Surface Analysis (Krumbein, 1959). The model consisted in combining the least-squares Gauss equation with a generic polynomial of type:

$$t = A_{00} + A_{10}\,U + A_{01}\,V + A_{20}U^{2} + A_{11}\,UV + \ldots + A_{pq}U^{p}V^{q} \qquad (2.4)$$

where t represents the trend component (e.g. a larger wavelength geophysical anomaly) of a variate X in $(U,\ V)$ space. A general relationship considers ε as an additional component of X:

$$X = t + \varepsilon \qquad (2.5)$$

suggesting that the roughness of the real dataset is also controlled by an additional component of random error and smaller scale oscillations (ε). The polynomial (t) is then a smoothing function that is used to generalise the real distribution of data.

Among the applications of *Surface Trend Analysis* it is worth noting the compilation of tables to perform calculations of linear coefficients in (2.4) using orthogonal polynomials (e.g. Oldham and Sutherland, 1955; Grant, 1957). These were used to remove the regional anomalies from gravitational field data. Miller (1956) used also least-squares to fit linear surfaces, and the method of averages to fit piecewise quadratic surfaces. His work pointed out that methodologies attempting to fit internal

points of regular grids (not at vertices) were better for geological applications, a case also illustrated below in the discussion of the Discrete Smooth Interpolation (DSI) method.

The progress of these methodologies was relatively slow because of the tedious calculations. Howarth (2001) gives a curious comparison reporting that in the 19th Century scientists such as Sabine had the advantage of human 'computers'- a group of trained soldiers was used to perform the calculations required. But to gain similar and even more 'extraordinary' computational power the advent of computers had to wait until the 1950s. After World War II, a period that stimulated the diffusion of statistics and promoted the development of computers for military applications, computers represented the solution to such tedious calculations, leading geologists to also start looking into automatic data processes (Krumbein, 1962). After computers entered the scene, the inversion of a $10 \times 10 \left[\boldsymbol{U}, \boldsymbol{V} \right]$ matrix (Krumbein, 1959; Howarth, 2001) became an easy task therefore accelerating interpolation methods and favouring their diversification, that finally led to modern geostatistics (Krige and Ueckermann, 1963; Matheron, 1970).

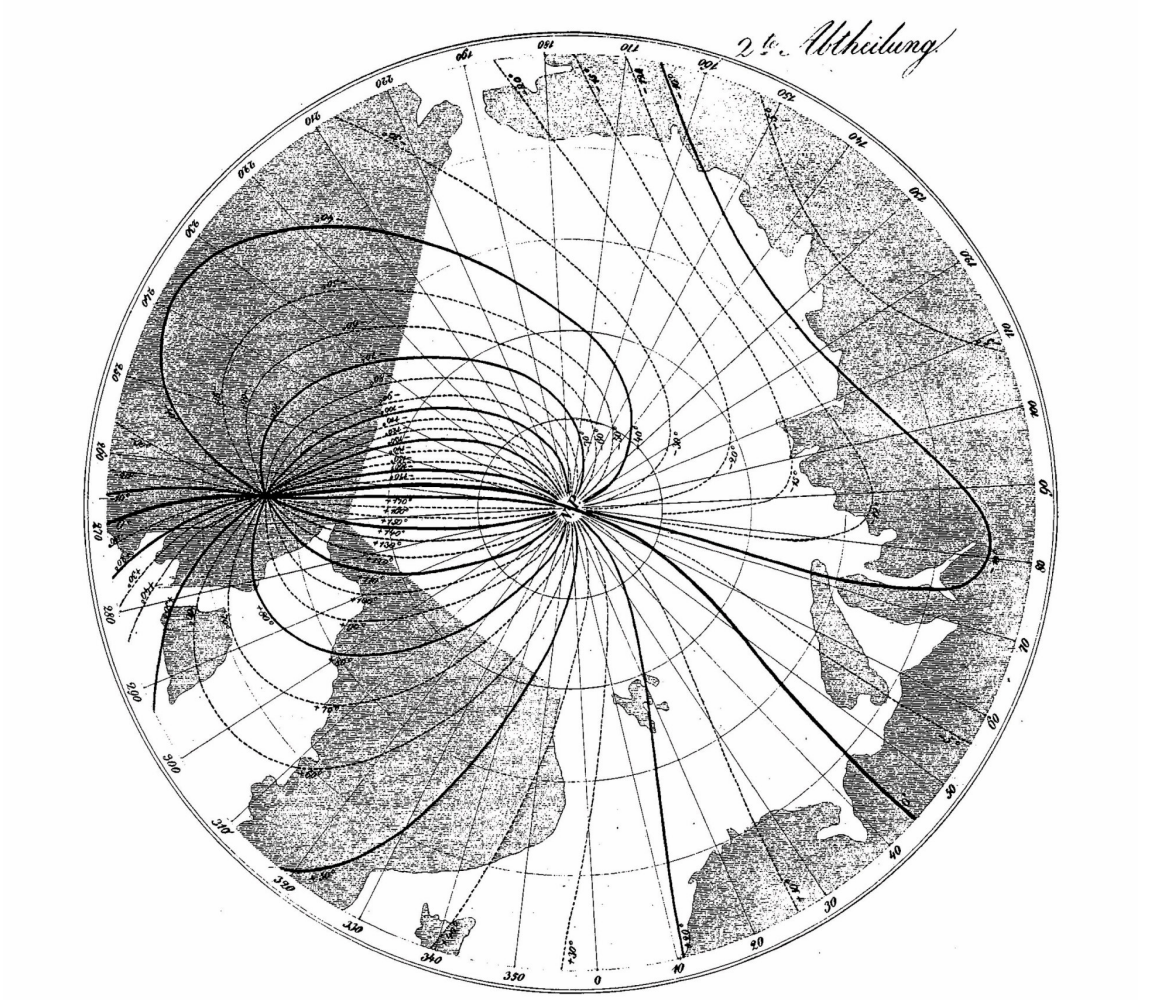

Fig. 2.4 Example of application of polynomial fitting to geophysical data. Isolines of magnetic declination of the Northern Hemisphere. Reproduced from Gauss and Weber (1839).

2.2.3 Geostatistics

The introduction of new methodologies was also due to the limitation encountered with polynomials, requiring more refined algorithms to resolve the excessive smoothness of this type of approximation. This led Griffin (1949), for example, to apply the method of moving averages to geophysical gravimetric data. The difference between this method and the use of polynomials lies in a generalisation based on averages of predefined neighbourhoods rather than a polynomial function that describes the whole spatial pattern. Howarth (2001) reports also an interesting application of these methodologies to Economic Geology problems such as gold estimation by a South African mining geologist (Krige, 1960). The most important discovery that this author reports is the autocorrelation function of gold assays - a spatial correlation among samples as a direct function of their distance from one another. This realisation led Krige to develop methodologies to correct grade estimations with the aid of regression analysis (Krige, 1951), also performing spatially weighted averages of ore blocks (Krige, 1966). Beside these early attempts to extend regression analysis at relatively small scales (e.g. mines, oil fields etc.), it was only after the substantial contribution of Matheron (e.g. Matheron, 1965) that the field of geostatistics found its independence as a modern, individual discipline in earth sciences. The work of Matheron was particularly important in mining applications although his contributions to geostatistics are largely accepted also outside

the geoscience world (Agterberg, 2001), reflecting the importance of his mathematical models. Matheron (1965) provides a theoretical framework for the early empirical models that accounted for both the interpolation of data, and more importantly for the uncertainty estimates associated with predictive models. Matheron was the first to use the term Kriging (in honour of Krige). Kriging is a type of interpolation based on two core algorithms. Firstly, a weighting algorithm aims to guess the value of a spatial point ($\hat{Z}_0$) on the basis of certain sphere of influence, similar to IDW (Inverse Distance Weighting) methods (see Bonham-Carter, 1994). Kriging equations contain a sample of the population of data with known variables (Z_i). Usually the sample can be represented as a cluster of points in space, occurring at variable distance. These need to be weighted accordingly. The relationship is then of the type:

$$\hat{Z}_0 = \sum_{i=1}^{n} w_i Z_i \qquad (2.6)$$

where w_i is a weighting coefficient that ranges from 0 to 1 (to avoid normalisation otherwise adopted in IDW methods);

Secondly an algorithm is needed to determine the level of uncertainty in the estimation of the w_i coefficients. This is because the calculation of these coefficients is function of the spatial variability of the dataset, relying on two types of covariance:

$$w_i = \frac{d}{C} \tag{2.7}.$$

Within this equation (d) is a linear vector that represents spatial 'covariances' between each Z_i and $\hat{Z}_0$ whereas (C) is a vector expressing the covariance among all the couples Z_i. These relationships can be expressed in compact form using the matrix notation as follows:

$$\begin{bmatrix} w_1 \\ \cdot \\ \cdot \\ w_n \\ \mu \end{bmatrix} = \begin{bmatrix} C_{10} \\ \cdot \\ \cdot \\ C_{n0} \\ 1 \end{bmatrix} \begin{bmatrix} C_{11} & C_{12} & \cdot & C_{1n} & 1 \\ \cdot & \cdot & \cdot & \cdot & \cdot \\ \cdot & \cdot & \cdot & \cdot & \cdot \\ C_{n1} & C_{n2} & \cdot & \cdot & 1 \\ 1 & 1 & \cdot & 1 & 0 \end{bmatrix}^{-1} \tag{2.8}$$

The term μ is a dummy number (Lagrange multiplier) used to rescale the weights in the range (0,1). (d) and (C) represent a measure of the dispersion, distance and spatial autocorrelation of a selected variable. Note that kriging uses multiple parameters to compute the weights, but these are measured on 'internal properties' of the same dataset and do not rely on other 'external' parameters (e.g. the relationship to other variables). In general terms the covariance C is expressed as a measure of spatial association between two variables for a sample (n):

$$C = \frac{1}{n}\sum_{i=1}^{n}\left(X_i - \overline{X}\right)\left(Y_i - \overline{Y}\right) \tag{2.9}$$

with *X, Y* as spatial coordinates. An analogous relationship is more commonly adopted to construct semi-variograms that are the most widespread tool in mining applications (e.g. Houlding, 1994). Usually such plots consider the moment of inertia versus the distance between couples of points (lag). The moment of inertia (γ) is defined as:

$$\gamma(h) = \frac{1}{2n}\sum_{t=1}^{n}\left(Z_t - Z_{t+h}\right)^2 \tag{2.10}.$$

The mathematical relationship is similar to equation (2.9) except that in this case the lag (h) is externally chosen and is regularly spaced to obtain the variogram. This autocorrelation function is based on a single variable and provides the degree of correlation between a central point Z_t positioned in t and any other point in the chosen neighbourhood ($t + h$). Both $C(h)$ and $\gamma(h)$ can be used to construct an experimental variogram that can be fitted with a mathematical model. Commonly, spherical or exponential curves are used to characterise the signal (Isaaks and Srivastava, 1989; Houlding, 1994). These equations are represented by a linear system of equations as

shown for different mathematical fitting models in Figs. 2.5a, b, c. The equations contain a series of coefficients that are used to fit the shape of the variogram and are also meaningful to their interpretation. For instance, in Fig. 2.5a the *spherical* model (Matheron, 1965) is represented by four coefficients: (s) is the *lag* or sample distance; (a) represents a limit after which the correlation starts vanishing; (C) is the variogram *sill,* a range of spatial association $\gamma(s)$; (C_0) is the *nugget effect*, the noise or background signal. Once the model is representative of the region of interest it can be applied to neighbour domains where the experimental autocorrelation is unknown. The three coefficients (a, C, C_0) are used then to obtain the covariance for each point within the chosen region allowing the definition of the w_i and therefore leading to the solution of equation (2.6). The interpretation of the variogram is however complex because of its variability as a function of the orientation of the region of interest and also as a direct function of the overall trend of the dataset. Bonham-Carter (1994) remarks that the fluctuation in the data can be of different scales and it is convenient to distinguish the trend (regional fluctuations) from the signal (the parameter of interest) and the noise. This can be done using methods such as Trend-Surface analysis. Kriging works in agreement with Agterberg (2001) only for stationary conditions and also for normal distributions (Houlding, 1994). The data are commonly pre-processed to respect these statistical constraints. A recent development is *Universal Kriging* that is essentially a combination of the above mentioned methodologies. Other types of kriging are also used for particular

purposes. For instance *Indicator Kriging* shares analogies with Bayesian modelling (Chapter 3), because it is used to evaluate the probability of meeting a certain threshold parameter chosen *a priori*, and also has similar data processing (reduction to Boolean data format).

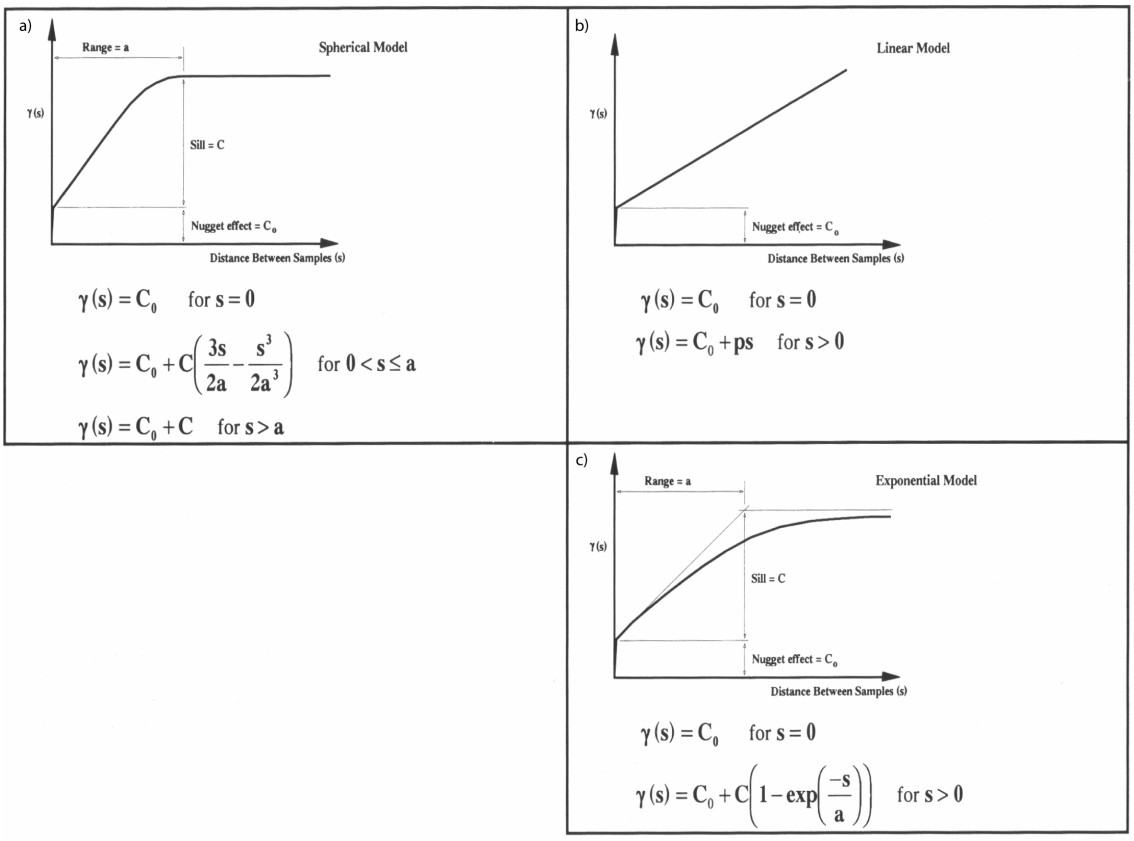

Fig. 2.5 Example of variogram plots showing respectively: (a) Spherical; (b) Linear; and (c) exponential model. Linear systems of equations of fitting curves are also included (see text for coefficients definitions), adapted from Houlding (1994).

Beside the diversification of kriging techniques, progress in geostatistics has also favoured the application of regression methods in alternative directions. One of the fields that gained progressive importance is the three-dimensional modelling used to simulate geological and biological objects. The need for a 3D representation of geologic themes has stimulated the development of specialised algorithms. For example Mallet (1989) proposed a discrete smoothing approach (DSI) to interpolate triangulated surfaces, which are often complex to handle with common tools such as spline based algorithms if datasets are geological. In a general sense the method provides a similar result to kriging interpolation (Mallet, 1989) although it is used to fit geometries rather than to predict ore grades. DSI and other algorithms were implemented in GoCAD, a software compiled in originally in C, but subsequently further developed in C++ language, at the University of Nancy (France).

Probabilistic regression models (Agterberg and Robinson, 1972; Tukey, 1972) were derived from mining and oil search applications. These more risk averse regression tools had the objective of answering the needs of exploration geologists when dealing with multivariate systems. The method consisted in rationalising the information in Boolean logic [0, 1] format that was particularly suited for digital computers, and allowed the combination of evidence. Data were organised in bi-dimensional format such as raster tables or grids representing the spatial distribution of a certain geological indicator (e.g. the geochemical distribution of an element). Regression curves were then fitted to each

variable and combined with a linear regression model. In an alternative to these early models Tukey (1972) suggested the use of logistic functions to ensure a range of probability (π) constrained in the [0, 1] interval (a definition of probability is given in the forthcoming section). The logistic function can be expressed in a general form as follows (Sahoo and Pandalai, 1999):

$$logit(\pi) = \beta_0 + \beta_1 x_1 + \beta_2 x_2 + \ldots + \beta_p x_p \quad (2.11)$$

π is expressed as the sum of contributions of different linear coefficients that can be represented by a linear vector $X_i = [x_1, x_2 \ldots x_p]$. The coefficients β_p reflect the slopes of each variate except for β_0 which represents the intercept of the regression line. The equation can be arranged in exponential fashion as follows to obtain the cell probability:

$$\pi_i = \frac{e^{X_i' \beta}}{1 - e^{X_i' \beta}} \quad (2.12)$$

Logistic regression, in contrast to kriging, makes use of multiple 'independent' variables rather than relying on different properties of the same variable (covariances) to provide estimates in the unknown region. Logistic equations of probability are also used in Weights of Evidence modelling. Favourability mapping methods (including Predictive

Neural Networks) are tools that find their root in Bayesian reasoning (e.g. Harris and Pan, 1999). They work as "trained networks" in which pairwise correlation (mineral deposits against other evidential themes) is used to adjust the weights (like the neural reinforcement of synapses), performing predictions where the correlations are verified.

As seen the progress brought firstly by analogue and then digital computers has contributed to a wide diversification of regression techniques. In part this has contributed to the development of relatively new ways to deal with geological problems. Computer simulation is certainly one of them. Among the diversification of mathematical models discussed so far computer simulation is one of the most actual, and represents in a certain way also a philosophical advance in the scientific approach.

2.2.4 Computer simulations

The use of simulation in the scientific sense has a fairly recent origin. It was firstly implemented in the 1940's by John von Neumann, who applied Monte Carlo Analysis in dealing with problems related to the shielding of nuclear reactors (Harbaugh and Bonham-Carter, 1970). The experimental approach in this case was rejected in favour of simulation because of the expenses and hazard involved. However, it is after the advent of digital computers in the 1950s that simulation, as it is conceived in modern applications, became relative common practise among economists, mathematicians and

later also among geologists. Perhaps one of the first geological applications is the work of Briggs and Pollack (1967), a digital simulation of evaporite sedimentation that solved partial differential equations by the Gauss-Seidel point iterative method on a high speed digital computer. The mathematical model allowed plotting of fluid flow vectors and also definition and graphic visualisation of spatial variability of salt concentrations across a bi-dimensional reconstruction of an epeiric basin in Michigan. The example is also part of an instructive chapter of 'Computer Simulation in Geology' (Harbaugh and Bonham-Carter, 1970), a book considered at least a decade ahead of its time (Merriam, 2004). The work of Brigs and Pollack (1967) concludes that statistical approaches are useless when dealing with a well known system modelled efficiently by deterministic methods (in this case dynamic simulation based on partial differential equations). However, laws of generalisation such as the Laplace equation (see below) have limited applicability- they work diligently only if the model is simplistic and integrable. In this context Nicolis (1995) reports that since the 1950s, physicists begun to realise (at least from a mathematical perspective) that most natural systems are non integrable, leading to *Hamiltonian chaos*. The evidence of a limit in the deterministic approach is also remarked in the problem of the particle/wave dualism of Heisenberg. Only adopting the concept of statistical distributions of Schrödinger was it then possible to define in a probabilistic manner the position and energy of an electron revolving around the nucleus of an atom. Physical experiences suggest therefore that deterministic models are

somehow confined to a partial solution. Probably a hybrid methodology may be more appropriate (i.e. chaos theory).

To summarise, the reviewed history of least-squares methods and the diversification of mathematical approaches (Fig. 2.6a, b, c) to model natural systems illustrates that scientific methodology had few major revolutions. Among them of notable importance are the establishment of experimental science and the advent of computers. The mathematical models adopted in this thesis offer some practical perspectives of the advantages that such revolution has brought to the geological world. Both statistical and deterministic applications are presented, and also they explore how the computer can be of use to the geologist at present. The meaning of usability can be evinced from Krumbein (1962) who foresaw computers as machines that *store* data, *integrate* data but also *think* as geologists do.

In this thesis then axiomatic logic and computer applications are implemented at different spatiotemporal scales, to solve geological problems in a similar manner to our scientific ancestors although in a more privileged technological age.

Fig. 2.6 Diversification of quantitative applications to geology in the 60s. (a) applications to the various geological sub disciplines; (b) time of entry of computer application in stratigraphy; (c) application of Markov models. Adapted from Krumbein (1969).

2.3 Mathematical models and computer software used in the Lawn Hill Region

The work presented here focuses on three major types of mathematical models: (1) Bayesian modelling adapted to a mineral exploration case; (2) Discrete Smooth

Interpolation approach used to model geological objects; (3) Fast Lagrangian Analysis of Continua used to model the coupling of fluid flow and deformation in 2D and 3D space. The first two models represent a derivation of regression analysis, whereas the third involves computer simulation. Even though the core chapters will address more specific aspects of the background of computational applications, here some general theory is considered.

2.3.1 Elements of probability

As seen computers not only can store and process a large amount of information (e.g. Hayes, 2002), they can also make inferences and provide predictive outputs. Statistical theories simulating human intellect are also used to make estimates of the uncertainty in risk analysis. Therefore AI (Artificial Intelligence) applications can be used more confidently in the making-decision process. This type of software is usually based on probabilistic laws composed of logical axioms (Agterberg, 1974; Haken, 2004). Elements of probability introduced here serves as basic theory for the more advanced treatment of Weights of Evidence modelling theory (Chapter 3).

2.3.1.1 Definition of probability

One way of looking at the meaning of probability is to consider the simple example of coin tossing, the simplest example of a chance mechanism corresponding to a binomial distribution [1, 0] (e.g. Bernoulli, 1954). The experiment involves tossing of a coin for a certain number of times representing the sampling of a population (a certain number of heads or tails is counted). When sufficient knowledge is available it can be concluded that there is a 50% probability to obtain one of the two states considered, $P = \frac{1}{2}$. If multiple averaging during coin tossing is performed (considering head as one and tails as zero) it is realised that the mathematical average progressively moves towards $P = \frac{1}{2}$, reflecting the likelihood ratio of the two possible states of equilibrium (*A, B*). A similar experiment can be undertaken using a dice, but in this case the number of possible states is 6, hence $P = \frac{1}{6}$.

A formal definition of probability is given: *The probability of an event is an abstraction of the idea of the relative frequency by which this event occurs in a sequence of trial measurements during a given experiment* (Agterberg, 1974).

Comparing the two examples some additional considerations can be drawn: the frequency of distribution is inversely proportional to the number of states of equilibrium (equal likelihood) allowed by the system (Haken, 2004). The two experiments show that

the probability function has a random, oscillatory behaviour although the fluctuation is always positive ($P \geq 0$) for each defined set A of the sample population of countable values, defined as ω.

2.3.1.2 Addition and multiplication of probability

The experiments and considerations made suggest that the sum of the probabilities is always equal to one, $P(\omega) = 1$, provided that each set is independent from one another, $A \cap B = 0$. The generalisation of these axioms suggests that the probability of a certain number of states is equal to the sum of the probabilities of each independent state. To verify this rule, the dice example can be used to calculate the probability of obtaining an odd number, which is $P = \frac{1}{2}$. As seen each state (*A, B* …) has a probability $P = \frac{1}{6}$. Knowing that, it can be easily verified that the probability is function of the number of degrees of freedom (Haken, 2004, see also example presented in Fig. 2.7a).

$$P\left(A \cup B\right) = P(A) + P(B). \tag{2.13}$$

Another fundamental operation (especially in Bayesian modelling) is the multiplication of probabilities defined also as *joint probability*, a concept useful to

describe the interrelationship among the probability functions of multiple variables. The simplest case is a bi-variate situation with $P(X)$ and $P(Y)$, with X and Y considered as random stets of variables (x_i, y_j). To verify that

$$P\left(X=x_i\,,\,Y=y_j\right)=P\left(X=x_i\right)P\left(Y=y_j\right) \tag{2.14}$$

an example of two layers of data in binary format is considered (Fig. 2.7b). Each layer is subdivided in a series of parallel rows and columns holding a random distribution of binary pixels. Each pixel can be white or black [0, 1]. The layers have equal size and also same number of rows and columns therefore they perfectly overlap. A finite number ($k+1$) of possible combinations (x_i, y_j) can be defined as a function of the k-layers. Using a Boolean operator "AND" each overlapping couple of pixels is multiplied to obtain a new layer. To assess the probability of finding a black pixel for each layer it can be demonstrated that for instance $P\left(X=x_b\right)=\frac{x_b}{x_{tot}}$; this is true also for all the other layers. It can be therefore proved that the probability of a black pixel in the third layer $P\left(Z=z_b\right)=\frac{z_b}{z_{tot}}$ is equal to the multiplication operation $\left[P\left(X=x_b\right)P\left(Y=y_b\right)\right]$. In other words calculating the $P(Z)$ by counting the black pixels on the Z layer or multiplying the probabilities of the two layers (X,Y) gives the same result.

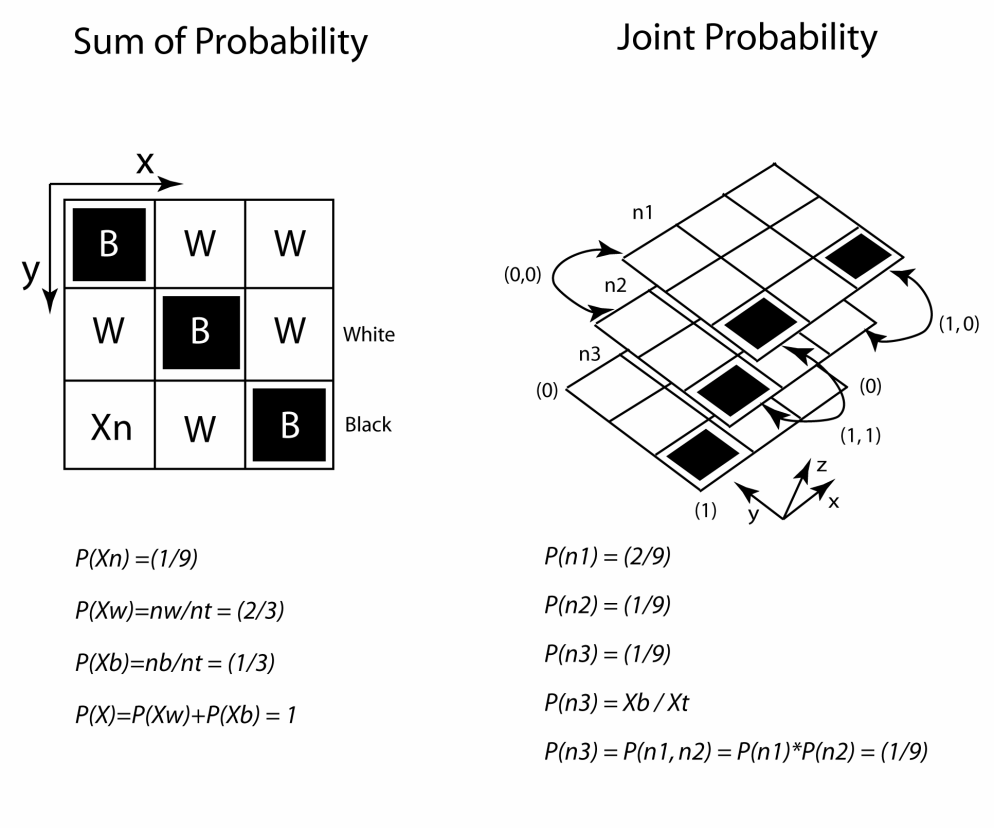

Fig. 2.7 Diagram presenting the concepts of addition and multiplication of probability (joint probability). (a) Nine cells model with black and white cells. Knowing that probability of each state is (1/9) it can be demonstrated that the sum of the probabilities for each individual state gives one. (b) Joint probability of multi-layer model considering the multiplication of two layers (n1, n2) giving n3 (see text for discussion).

2.3.1.3 Distribution, normal distribution and confidence interval

The probability distribution of a sample is a partial figure of the probability distribution of the population. To examine how the density of distribution varies it is convenient to explore a sampled population (ω) considering a number of well defined

subsets represented by equivalent intervals h_n of the random variable (X) as shown in the histogram of Fig. 2.8a. These subdivisions can also be considered as a series of probability intervals $P\left(h_k \le X \le h_{k+1}\right)$ because of the initial consideration. This axiom can be generalised for a subset A in the form:

$$P(X \in A) = \sum_{v_n \in A} P_n \tag{2.15}$$

where v_n are distinct values of the subset A belonging to $X(\omega)$ and P_n are their elementary probabilities $P\left(X = v_n\right)$ (Fig. 2.8b). An alternative approach to explore the density $P(X)$ variation for a discrete countable (ω) is also the definition of a cumulative probability function $F_X(X)$ (Fig. 2.8c) where the subset A simply represents and interval between $-\infty$ and x hence:

$$F_X(x) = P(X \le x) = \sum_{v_n \le x} P_n \tag{2.16}$$

The elementary probability (P_n) is clearly a discrete parameter in the histogram of Fig. 2.8a. However, it can be generalised to a piecewise continuous function $F_X(x)$ that is integrable in its interval of definition:

$$F_X(x) = \int_{-\infty}^{x} f(x)\,dx \tag{2.17}$$

The generalisation holds for a subset *A* leading to:

$$P(X \in A) = \int_A f(x)\,dx \tag{2.18}.$$

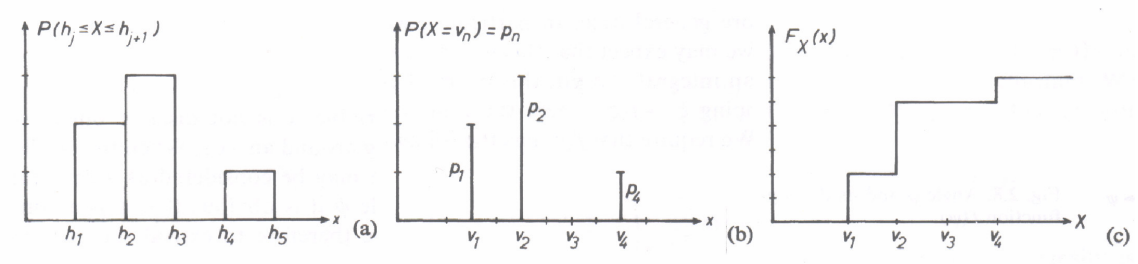

Fig. 2.8 Probability (*P*) of finding a set between h_j and h_j+1. (a) Histogram representing the distribution of samples. (b) Probability measure, the number of individuals v_i per each set A. (c) Distribution function $F_X(x)$ representing the cumulative proportions depending upon the number of sets considered (adapted from Haken, 2004).

The last two definitions (2.17, 2.18) suggest that a sampled population (ω) can be approximated by a mathematical function *f*(*x*). One example that is the most common distribution type is the Gaussian normal distribution. Following Agterberg (1974) the probability distribution *f*(*x*) and its cumulative function *F*(*x*) can be defined as follows:

$$f(x) = \frac{1}{\sigma\sqrt{2\pi}} \exp\left\{-\frac{1}{2}\left(\frac{x-\mu}{\sigma}\right)^2\right\} \tag{2.19}$$

and

$$F(x)=\left(\frac{1}{\sigma\sqrt{2\pi}}\right)\int_{-\infty}^{x}\exp\left\{-\frac{1}{2}\left(\frac{x-\mu}{\sigma}\right)^{2}\right\}dx \tag{2.20}$$

where σ is the standard deviation from the mean (μ) and x is an ordinary variable of $f(x)$. Commonly these equations can be simplified by defining a normal random variable z equal to $\left(\frac{X-\mu}{\sigma}\right)$ with mean equal to zero and standard deviation of one. Then $f(z)$ and $F(z)$ can be written as:

$$\phi(z)=\frac{1}{\sqrt{2\pi}}e^{-\frac{1}{2}z^{2}} \tag{2.21}$$

and

$$\Phi(z)=\frac{1}{\sqrt{2\pi}}\int_{-\infty}^{z}e^{-\frac{1}{2}z^{2}}dz \tag{2.22}$$

This rescaling (2.21, 2.22) translates the population mean (μ) at zero and sets the inflection points of the Gaussian at σ (for a normal population). Combining equation (2.17) and (2.18), $P(X \leq z) = \Phi(z)$.

Choosing Z [-1, 1] an interval is defined in which a random sample X has $P(-1<Z<1) = \Phi(1) - \Phi(-1) = 0.841 - 0.159 = 0.682$, considering also that $z = \left(\frac{X-\mu}{\sigma}\right)$ and rearranging $P\left(-\sigma+\mu<X<\sigma+\mu\right) = 0.682$. The solution suggests that there is a chance of 68% to sample within σ. The same formula can be extended to determine the probability to sample between 2σ or 3σ, respectively with a probability 0.954 and 0.997. Otherwise the use of a z value of 1.64 or 1.96 is widespread. Agterberg (1974) extends this approach suggesting that it is possible to use the concept of confidence interval to obtain a standard test (z-test of significance) for the measure of the normality of a population. To formulate the test it is necessary to follow three steps: (1) establish a null-hypothesis H_0; (2) define a significance limit and (3) compute the average $\overline{x}$ and compare it with the region of acceptance. The main distinction with the previous case is that a real population is sampled with mean (μ_0) that could be different or equal to the Gaussian mean (μ). The H_0 test proposes then to verify if $\mu_0 = \mu$, however commonly this condition is too restrictive. A range of acceptance firstly redefines the z value as:

$$z = \frac{\overline{x} - \mu}{\sigma \sqrt{n}} \tag{2.23}$$

In this case the average $\overline{x}$ is used because it is representative of the sampled real population. The relationship can be also expressed as modulus and a significance limit of 1.96, as follows:

$$|z| = \left| \frac{\overline{x} - \mu}{\sigma \sqrt{n}} \right| < 1.96 \tag{2.24}$$

The condition (2.24) suggests that for large z, H_0 is rejected. Rearranging and considering that μ_0 may not be defined depending upon available sampling it is however possible to define a confidence interval for the average $\overline{x}$ with probability:

$$P\left(\overline{x} - 1.96 \frac{\sigma}{\sqrt{n}} < \mu < \overline{x} + 1.96 \frac{\sigma}{\sqrt{n}} \right) = 0.95 \tag{2.25}$$

If the (2.25) is valid then the test is passed because the population has a mean value $\mu_0 \cong \mu$ and therefore approximates a normal distribution. However, with a level of significance $\alpha = 0.05$ there is still a 5% chance that the sample average will be rejected

because of the error limit considered. In other words firstly it is ensured that the sample resembles a normal distribution, but if the sample has several x_i that fall outside the error limit the hypothesis would be rejected even if the sample effectively relates to a normal population represented by a random variable X.

2.3.1.4 Mathematical expectation and variance

The two model parameters most commonly used in probabilistic approaches to estimation are the mean or "expected value" of the random variable and its variance (Isaaks and Srivastava, 1989). These are also defined as Moments, an integral form to express the mean and standard deviation of a piecewise continuous function. It is therefore convenient to start analysing the concept of expectation (mean) from a discrete perspective to then define it in integral form. It will be shown then how the standard deviation can be calculated, for similar reasons, from the mean.

Returning to the example of the dice, six states with equal probability of occurrence were observed. Performing the simple mathematical average $\overline{x}$ of a sample of several throws (n) of value v_i, this is given by:

$$\overline{x} = \frac{1}{n}\left(\sum_{i=1}^{n} v_i\right) \tag{2.26}$$

The probability of occurrence based on the total number of throws can be expressed as $p_n = \frac{v_{in}}{n}$ where v_{in} is the number of outcomes for a certain state. Therefore, the mean can also be expressed as the weighted average of the outcomes for each possible class multiplied by the relative probability:

$$E(X) = \sum_n v_n \, p_n \tag{2.27}$$

where $E(X)$ is the expectation and v_n represents each possible class of outcomes (six for the dice). The expectation can be evaluated also for continuous functions $f(x)$ of random variables generalising as follows:

$$\mu_1 = EX = \int v f(v) \, dv \tag{2.28}$$

also defined as the first moment.

The second moment in contrast is used to define the variance (σ^2) of the mean of a continuous function. The variance of a discrete random variable is expressed as:

$$\sigma^2 = \frac{1}{n}\sum_{i=n}\left(v_i - \overline{v}\right)^2 \tag{2.29}$$

For similar reasons leading to (2.27) equation (2.29) can incorporate the elementary probabilities p_n as follows, however in this case it is convenient to refer to the definition of the moment about the mean (see Agterberg, 1974). The discrete equation follows:

$$\sigma^2 = \sum_n (v_n - \mu)^2 \times p_n \tag{2.30}$$

In integral form for continuous functions the same considerations are valid and lead to:

$$\sigma^2 = \int (v - \mu)^2 f(v)\, dv \tag{2.31}$$

Equation (2.30) can be imagined as a histogram with bins oscillating around a mean value weighted using the elementary probabilities.

2.3.2 GoCAD and the DSI algorithm

The mathematical models examined in this section are mostly used in geometrical modelling and were implemented to reconstruct regional and deposit scale 3D models of the Century deposit. To construct a 3D structural model of this mineralised body, the software package GoCAD was used. GoCAD is suited to model natural objects, whereas traditional CAD platforms are based on software engines that use polynomial algorithms (e.g. Bézier, 1974; Barnhill, 1985; Farin, 1988) created to answer the exigencies of industries that make manufactured objects. These two approaches are different in the sense that modelling geological objects has to respect the data imported during the preliminary phase of model construction. CAD applications have as a primary aim the creation of models with smooth and nice curves, surfaces, and volumes. As a consequence it is not easy to integrate geological datasets in common CAD software and the use of GoCAD becomes obvious. The software has been developed within a consortium which is widely open both to the industry and universities around the world. Several collaborative organisations (e.g. pmd*CRC - Predictive Mineral Discovery Cooperative Research Centre) are interested in the type of geomodelling proposed by GoCAD and want to use and/or contribute to the development of this new technology.

Mallet (2002) presents a comprehensive description of the mathematical algorithms behind GoCAD, in particular discussing the DSI (discrete smooth

interpolation algorithm) that represents the core of this application. Recently the software has become more a collection of several modules that allows import/export of a number of formats and also different types of interpolation functionalities. The GoCAD technology prefers to adopt a discrete method that is close to a "finite elements" approach, rather then use a parametric approach based on continuous polynomial functions. Discrete modelling methods are well known and represent an easier way to mathematically treat geological problems (Mallet, 2002).

2.3.2.1 Topology of an object

The topology represents the arrangement in which the nodes of a curve, surface or solid are connected to each other. Thus object topology can be described using a mathematical function of two variables $\xi(\Omega, N)$ where Ω is a set of nodes used to describe the object. Each node is identified by its rank order: $\Omega = \{1,2,\ldots., \alpha,\ldots.,M\}$. N is defined as an application from Ω into a subset of Ω such that

$$\{\beta \in N(\alpha)\} \Leftrightarrow \{\beta \text{ can be reached in at most } s(\alpha) \text{ steps from } \alpha\}.$$

This means that a generic node α is part of Ω and is surrounded by neighbours (β_n nodes), and that the topological relationship existing between α and its neighbourhood can be expressed as a function $N(\alpha)$, which is called neighbourhood operator (Fig. 2.9).

Fig. 2.9 Neighbourhood diagram N(α) from Mallet (2002), representing a discrete domain of a point in space with a central point (α) surrounded by a series of points (β) representing a local subset interconnected by a polygonal mesh. This set represents the minimum scale at which the DSI interpolation operates s(α) = 1.

The notion of a discrete topological model can be used to approximate the topology of any geological object. Some examples are: (1) *geological horizon* or fault (surface) as a set of adjacent triangles; (2) *geological body* (solid) as a set of adjacent tetrahedrons; (3) *geological cross-section* (curve) as a set of adjacent segments; (4) *geological layer* (solid) as a regular curvilinear or rectilinear grid. The vertices of the triangles are equal to

the nodes of $\xi(\Omega, N)$, while the edges partly define the topology of these objects (Fig. 2.10).

Fig. 2.10 Examples of objects approximated by a discrete model. (a) Triangulated surface; (b) Tetrahedral solid filling a geological horizon; (c) Polygonal curves; (d) Faulted curvilinear grid (adapted from Mallet, 2002).

2.3.2.2 Concept of discrete model

The notion of a topological discrete model has to be further extended, because a discrete topological model does not take into account the properties of the represented geological objects and the possible constraints that might be applied to them. Hence, the

function $\xi(\Omega, N)$ has to be included in a generic function $M^n(\Omega, N, \varphi, C)$ where φ is a set of functions $\varphi(\alpha)$:

$$\varphi(\alpha) = \{\varphi^1(\alpha), \ldots, \varphi^v(\alpha), \ldots, \varphi^n(\alpha)\} \qquad \forall\ \alpha \in \Omega \tag{2.32}$$

$\varphi(\alpha)$ represents a series of properties of an object node α. For example, the spatial location of a node is defined from the following components of $\varphi(\alpha)$:

$$\{\ \varphi^x(\alpha), \varphi^y(\alpha), \varphi^z(\alpha)\ \} \tag{2.33}.$$

C is a set of constraints that can be split into three subsets:

$$C = C^{\cong} \cup C^{=} \cup C^{>}; \tag{2.34},$$

where $C^{\cong}$ is the set of "soft" equality constraints that have to be honoured in a least square sense, $C^{=}$ is the set of "hard" equality constraints that have to be strictly honoured, and $C^{>}$ is the set of "hard" inequality constraints that have to be strictly honoured.

These subset functions represent three ways to impose a property $\varphi^{v}(\alpha)$ on an object and as a consequence these subsets have different control (e.g. on its topology). Constraints and properties, as seen below, are expressed by similar mathematical expressions. Applying a constraint to a generic model and subsequent interpolation usually forces the properties to adapt to the constraint. A simple example of constraint can be envisaged as a set of control points that are used to define the topology of a surface. Using the GoCAD GUI (Graphic User Interface) functionalities it is possible to fit a surface to the selected control points using them as a *control point* constraint.

2.3.2.3 Discrete Smooth Interpolation approach

The Discrete Smooth Interpolation method (DSI) has been designed specifically for interpolating the function φ of a discrete model $M^n(\Omega, N, \varphi, C)$, while respecting all the constraints $c \in C$. Here, only soft constraints $c \in C^{\cong}$ and a subset C^L of $C^{=}$ are implemented to give an easier introduction to this mathematical formulation. A scalar continuous function φ defined within the segment $\overline{\Omega} = [1, M]$ and letting Ω be the set of nodes corresponding to the regular sampling of $\overline{\Omega}$ with a step equal to 1: $\Omega = \{1, 2, \ldots, \alpha, \ldots, M\}$. In Fig. 2.11 the nodes $\alpha \in \Omega$ correspond to the white points, while the black points correspond to some given data points $\{l, \varphi(l) : l \in L\}$ to be interpolated and associated

with a given subset L of Ω. For this purpose, a classic method (Farin, 1988) consists in looking for a spline function φ, minimising the "global roughness" $\breve{R}(\varphi)$ such that:

$$\breve{R}(\varphi) = \int_{\Omega} \mu(x) \cdot \breve{R}\left(\varphi | x\right) dx \qquad (2.36),$$

with: $$\breve{R}\left(\varphi | x\right) = \left| \frac{d^2 \varphi}{dx^2} \right|^2 \qquad (2.37).$$

In this expression, $\mu(x) > 0$ is a given "stiffness" function (that can be taken constant and equal to 1), while $\breve{R}\left(\varphi | x\right)$ can be considered a measure of the "local roughness" of φ at each point $x \in \Omega$ considering that:

$$\overline{\varphi}(x) = \frac{\varphi(x-1) + \varphi(x+1)}{2} \qquad (2.38).$$

Then, as suggested in Fig. 2.11, it can be verified that a finite-difference approximation of $\left|\frac{d^2\varphi}{dx^2}\right|$ is such that:

$$\left|\frac{d^2\varphi}{dx^2}\right| \approx 2\cdot\left\{\overline{\varphi}(x)-\varphi(x)\right\} = \left\{1\cdot\varphi(x-1)+1\cdot\varphi(x+1)\right\}-2\varphi(x) \qquad (2.39).$$

The next section on numerical simulation gives an explanation of how finite-difference approximation works.

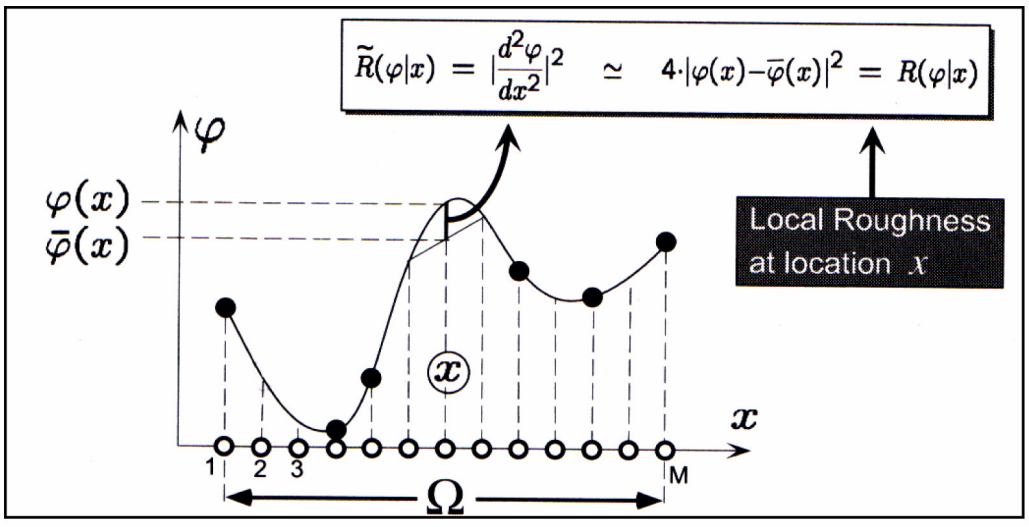

Fig. 2.11 Finite difference approximation using a spline function $\varphi(x)$ and relative local roughness/function $\tilde{R}(\varphi|x)$ representing the residual of $\overline{\varphi}(x)$ defined in a finite interval $\Omega[1, M]$. The objective of using a local roughness criterion is to minimise its value therefore reducing the residuals, similarly to the least square method, to obtain a better fit (adapted from Mallet, 2002).

If φ is a continuous periodic function with period equal to Ω the above approximation can be considered valid. Hence it follows that

$$\breve{R}\left(\varphi|x\right) \approx \left| \sum_{\beta \in N(\alpha)} v\left(\alpha,\beta\right) \cdot \varphi\left(\beta\right) \right|^2 \qquad (2.40),$$

where $v(\alpha, \beta)$ represents an arbitrary coefficient used to weight the magnitude of the variation of each component $\varphi^v(\alpha)$ of $\varphi(\alpha)$. For a detailed description on how to set the weighting coefficients refer to Mallet (2002) - here there is more concern with the result of this approximation. Thus defining $R(\varphi)$ as an approximation of $\breve{R}(\varphi)$ (global roughness), and

$$R(\varphi) = \sum_{\alpha \in \Omega} \mu(\alpha) \cdot R\left(\varphi|\alpha\right) \qquad (2.41)$$

with:

$$R\left(\varphi|\alpha\right) = \left| \sum_{\beta \in N(\alpha)} v\left(\alpha,\beta\right) \cdot \varphi\left(\beta\right) \right|^2 \qquad (2.42),$$

it can be concluded that $\breve{R}(\varphi) \approx R(\varphi)$. Minimising $\breve{R}(\varphi)$ or $R(\varphi)$ therefore holds approximately equivalent results (Mallet, 1989; Mallet, 2000; Mallet, 2002).

2.3.2.4 Discrete Smooth Interpolation algorithm

A discrete model $M^I(\Omega, N, \varphi, C)$ is considered here. In this case, φ has only one component, thus no distinction will be made between φ and φ^1. L and H are also considered as two complementary subsets of Ω such that (1) L = set of nodes $l \in \Omega$ where $\varphi(l)$ is known and represents a constraint; (2) H = set of nodes $h \in \Omega$ where $\varphi(h)$ is unknown. The set L is called the set of "Control-Nodes" and is associated with a particular subset C^L of the set of hard constraints $C^=$. The aim is to compute the values $\{\varphi(h): h \in H\}$ in such a way that the resulting function φ is "as smooth as possible" on $\xi(\Omega, N)$. The "control values" $\{\varphi(l): l \in L\}$ should be strictly honoured, and each of the constraints $c \in C^{\cong}$ should be respected as much as possible. For this purpose, it is necessary to quantify the local roughness $R(\varphi|\alpha)$ of φ in the neighbourhood of each node $\alpha \in \Omega$ and evaluate the degree of violation $\rho(\varphi|c)$ of each constraint $c \in C^{\cong}$ by φ as follows:

$$R(\varphi : \alpha) = \left| \sum_{\beta \in N(\alpha)} v\left(\alpha, \beta\right) \cdot \varphi\left(\beta\right) \right|^2 \quad (2.43),$$

$$R(\varphi : c) = \left| \sum_{\alpha \in \Omega} A_c(\alpha) \cdot \varphi(\alpha) - b_c \right|^2 \quad (2.44),$$

where A_c and b_c are coefficients that define the type of constraint depending on their value (soft, hard).

The function φ must be chosen to minimise $R^*(\varphi)$, the "general roughness" criterion:

$$R^*(\varphi) = \sum_{\alpha \in \Omega} \mu(\alpha) \cdot R\left(\varphi | \alpha\right) + \left(\phi \cdot \overline{\omega}\right) \sum_{c \in C^=} \overline{\omega}_c \cdot \rho\left(\varphi | c\right) \quad (2.45).$$

Equation (2.45) combines on its right side the local roughness and violation functions, but also considers the stiffness function $\mu(\alpha) > 0$ which modulates the importance of the local roughness $R\left(\varphi|\alpha\right)$ at node (α). $\overline{\omega}_c$ is a term that controls the relative weights of different constraints whereas $\left(\phi \cdot \overline{\omega}\right)$ is used to define a balance between the two sets of functions:

$$\sum_{\alpha \in \Omega} \mu(\alpha) \cdot R(\varphi|\alpha) \quad \text{and} \quad \sum_{c \in C^{=}} \overline{\omega}_c \cdot \rho(\varphi| c) \tag{2.46}.$$

From the mathematical formulation of Mallet (2002) we can conclude that the DSI approach treats complex problems as a discrete subset of simpler linear problems. Thus a degree of simplification is induced in the first part of this method (discretization), whereas in a secondary step a "minimum energy" principle is applied, aiming to reduce the "global roughness", which can be seen as the difference between the applied constraints and the unconstrained functions that represent the properties of an object. The use of constraints during the modelling phases of the Century deposit represented an excellent tool to define an accurate shape for horizons and faults and interpolate the grades on both two-dimensional and three-dimensional grid based models.

2.3.3 FLAC (Fast Lagrangian Analysis of Continua)

This section briefly introduces the core algorithms behind the explicit Lagrangian formulation adopted in FLAC, a program designed to run geomechanical simulations that was firstly developed by Peter Cundall in 1986 (Itasca, 2003, and further enhanced by CSIRO Exploration and Mining) to handle a wider range of geological problems including application to mineral deposit exploration. The software was used in this thesis

to model coupled deformation and fluid flow within 2D-3D geological scenarios that resemble the Century mineral system.

2.3.3.1 General description of FLAC

FLAC simulates behaviours of geological materials that undergo plastic flow during yield and it has been applied in many geological situations (Ord, 1991b, a; Ord and Oliver, 1997; Oliver et al., 1999; 2001; Ord et al., 2002; McLellan et al., 2004; Miller and Wilson, 2004; Oliver et al., 2006). Materials are represented by polyhedral elements within a two- or three-dimensional grid that can be adjusted by the user to fit the shape of the geological bodies to be modelled. Two versions of the software were utilised to perform numerical simulations both in 2D and 3D. The simulated materials can yield and flow leading to permanent deformation of the grid. Two numerical approaches represent the basis of the FLAC environment: (1) the explicit, Lagrangian calculation scheme and (2) the mixed-discretization zoning technique (Itasca, 2003). These mathematical models are used to ensure that plastic collapse and flow are modelled accurately. They also require less computational effort compared to FEM (Finite Element Models) because they avoid utilization of a large stiffness matrix to reach a final stable solution (Itasca, 2003). Additionally problems such as small time-step limitation and dumping (e.g. dissipation of kinetic oscillatory energy) are handled respectively by inertia scaling and automatic

damping functions (Itasca, 2003). In addition to the core algorithms based on the use of finite-difference approximation, which is perhaps one of the oldest numerical techniques used for the solution of sets of differential equations (given initial values and/or boundary values; Desai and Christian 1977), the software offers ten different constitutive models to simulate mechanical deformation of various materials:

(a) the "null" model;
(b) three elasticity models (isotropic, transversely isotropic and orthotropic elasticity); and
(c) six plasticity models (Drucker-Prager, Mohr-Coulomb, strain hardening/softening, ubiquitous-joint, bilinear strain hardening/softening ubiquitous-joint, and modified Cam-clay).

Each zone in a FLAC grid may have a different material model or property and also gradients or statistical distributions can be specified as well. Additional anisotropies can be introduced such as interfaces or slip-planes between two ore more portions of the grid to simulate for example a fault/fracture or other parallel bedding anisotropies. FLAC also incorporates the facility to model confined fluid flow and pore-pressure dissipation, and the full coupling between deformable porous solid and a viscous fluid flowing within the pore space. The fluid is assumed to obey the isotropic form of the Darcy's law. Both

fluids and grains in the porous solid are deformable. All zones in a model are assumed to be fully saturated; therefore it is not possible to simulate phreatic surfaces in FLAC.

2.3.3.2 Basics of the finite-difference method to solve differential equations

To briefly illustrate the fundaments of finite-difference approximation methods, reference is made to the book of Harbaugh and Bonham-Carter (1970). The book was written from a geologist's perspective therefore its simple and applied approach to basic mathematical concepts such as differential computation, represents an attractive way to understand the finite difference method in a general manner. Finite difference is used, for instance in FLAC, to obtain solutions of partial differential equations relative to motion and also to solve the constitutive laws (discussed in more detail below) both in a spatial and temporal scenario. The approach is also appealing for computer based implementation, because although the finite-difference approximation is a relatively simple method, it requires an elevated number of calculations (on the order of thousands if not millions).

Considering a simple example of an algebraic equation such as:

$$3x + 4 = 0 \tag{2.47}$$

The equation can be solved by manipulation obtaining $x = -\frac{4}{3}$. This example shows then that some equations can be easily solved without the need of any particular method, but this approach fails in other cases. Harbaugh and Bonham-Carter (1970) suggest for example that the only way to solve the equation that describes the wave motion from deep to shallow water settings in a sedimentary basin, is to use an iterative approach. The equation is the following:

$$l = L \tanh\left(\frac{2\pi h}{l}\right) \qquad (2.48),$$

where l and L are the wavelengths respectively at shallow and deeper depths and h is the water depth. Equation (2.48) cannot be solved with algebraic manipulation because of the occurrence of the term (l) on both sides. However, rewriting the equation in this form, introducing a new l_0 term:

$$l = L \tanh\left(\frac{2\pi h}{l_0}\right) \qquad (2.49)$$

allows exploration in an experimental way of the field of solutions for l considering an array of l_0 values that are selected trying to reach the condition $l = l_0$. Unfortunately this

approach is cumbersome when the field of solutions is characterised by multiple maximum values where $l=l_0$, because the equation may be satisfied by more than a single combination of independent variables. In this regard a number of mathematical approaches can be adopted to solve the problem, e.g. integration where possible or the finite-difference approximation examined here, or even more advanced tools such as genetic search based algorithms that look for the "fittest solution" in a search space (see Coley, 1999).

A differential equation can be ordinary or partial, depending on the number of variables and their relative derivatives. The order of a differential equation is defined by highest exponential derivation; here first and second order linear ordinary and partial differential equations are considered, as they are sufficient to introduce how the FLAC finite-difference approximation works.

Considering a simple example of ordinary differential equation of the first order:

$$\frac{dN}{dT} = rN \tag{2.50}$$

it is instructive to note that the relationship considers a first order derivative in time (T) of N individuals in a generic population, which is equal to N individuals multiplied by a

constant of proportionality (r). The relationship can be easily solved with integration as follows:

$$\int \frac{1}{N} dN = r \int dT \qquad (2.51).$$

Then solving algebraically the integration it is obtained: $\ln(N) = rT$. This equation can be also written for an interval of time [0, T] as follows:

$$N_t = N_o e^{rT} \qquad (2.52),$$

where N_0 is an initial value for the population and N_t represents its growth at time (t). Graphically this relationship is represented by an exponential curve as illustrated in Fig. 2.12. As already mentioned it is not always possible to solve an equation using algebraic approaches therefore here the same example can be alternatively solved using the finite-different quotient approximation (Nystrom's method).

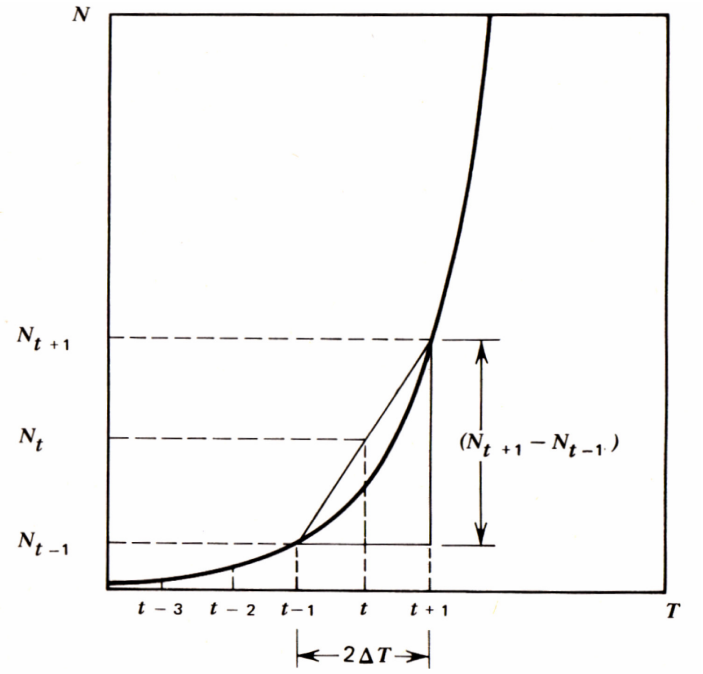

Fig. 2.12 Example of an exponential curve and relative intervals of discretization Δt illustrating the growth of a generic population (N). The growth value for an instantaneous time (t) can be estimated using the finite-difference quotient approximation (Nt+1-Nt-1)/2Δt. Adapted from Harbaugh and Bonham-Carter (1970).

The numerical solution of a differential equation can be obtained then transforming continuous derivatives into finite-difference quotients, hence:

$$\frac{dN}{dT} \cong \frac{\Delta N}{\Delta T} \qquad (2.53).$$

This approximation improves for smaller finite-difference intervals of approximation ($\Delta T \rightarrow 0$). In this regard this concept can be clarified selecting a mid point (*t*) (see Fig. 2.12) which seats at *t+1* and *t-1* from two extremes at ΔT giving:

$$\frac{dN}{dT} = \frac{N_{t+1} - N_{t-1}}{2\Delta T} \tag{2.54}.$$

Combining with (2.50) removes the differential term to provide an analytical solution to the differential equation of this type:

$$\frac{N_{t+1} - N_{t-1}}{2\Delta T} = rN_t \tag{2.55}.$$

This can be also rearranged as follows:

$$N_{t+1} = 2\Delta T r N_t + N_{t-1} \tag{2.56}.$$

Provided that an r = 0.5 is selected and also that ΔT = 1, this relationship can be further reduced to:

$$N_{t+1} = N_t + N_{t-1} \tag{2.57}.$$

It is then possible to compute a point of intersection of the function knowing two points at ΔT allowing then the construction of an approximate curve. If $\Delta T \mapsto 0$ the approximation will be more accurate, because the guessed extreme, using (2.57), will be closer to the known intersecting points. By analogy the same approximation holds if the derivation describes the rapidity of variation of a space variable. Therefore for first- and second-order derivations in bi-dimensional space (*x, y*) it is possible to write the following formulas of approximation:

$$\left(\frac{dy}{dx}\right)_j \cong \frac{1}{2\Delta x}\left(y_{j+1} - y_{j-1}\right); \qquad (2.58),$$

$$\left(\frac{d^2y}{dx^2}\right)_j \cong \frac{1}{2\Delta x}\left(y_{j+1} - 2y_j + y_{j-1}\right); \qquad (2.59),$$

where *j* represents a generic point on the curve. Once the finite-difference quotients have been calculated, as seen, a number of linear equations can be compiled to represent the field of solutions needed to describe the spatial variation of *x* and *y*. The coefficients *y*(*x*) will be obtained throughout an iterative process (e.g. Gauss-Seidel). However, the field of solutions depends also on the boundary values assigned, guessed before starting

the iteration. These values remain constant and are not updated during the progressive steps of iteration.

The finite-difference approach can be extended to more than a single variable introducing multiple derivations (partial derivatives) of a variable in respect of others, generalising then to a surface-based or volume-based space. Two examples of partial differential equations are given:

$$\frac{\partial^2 z}{\partial x^2} + \frac{\partial^2 z}{dy^2} = 0; \qquad (2.60),$$

$$\frac{\partial^2 \Phi}{\partial x^2} + \frac{\partial^2 \Phi}{dy^2} + \frac{\partial^2 \Phi}{dz^2} = 0; \qquad (2.61).$$

Equation (2.60) describes the spatial variation of a surface $z = f(x,y)$ in three-dimensional space, whereas (2.61) represents the Laplace equation that define the spatial variation of a generic function Φ in three-dimensional space $\Phi = f(x, y, z)$. The two examples are illustrated in Fig. 2.13a, b, c and d. To represent this type of function in a discrete manner, it is usually convenient to construct squared meshes projected in three-dimensional space or cubic voxels in the case of (2.61). The solution of the differential

equations can be obtained in a similar manner replacing the partial differential terms with relative finite-difference approximation terms as follows:

$$\frac{1}{\Delta x^2}\left(z_{i,j+1} - 2z_{ij} + z_{ij-1}\right) + \frac{1}{\Delta y^2}\left(z_{i+1,j} - 2z_{ij} + z_{i-1,j}\right) = 0 \qquad (2.62),$$

and for the Laplace equation considering $\Delta x = \Delta y = \Delta z$ leads to the following:

$$\frac{1}{\Delta x^2}\left(\Phi_{i,j-1,k} + \Phi_{i,j+1,k} + \Phi_{i-1,j,k} + \Phi_{i+1,j,k} + \Phi_{i,j,k-1} + \Phi_{i,j,k+1} - 6\Phi_{i,j,k}\right) = 0 \qquad (2.63),$$

the indexes [*i, j, k*] represent the direction in which the function Φ is approximated (see Fig. 2.13b, d). The (2.62, 2.63) can be used to derive a value of the functions z or Φ on a surface or in a volume represented by a finite number of cells identified by [*i, j, k*].

Similarly to the example of ordinary differential equations the search of the solution space is performed with an iterative approach. But this time the number of boundary values is represented by a neighbourhood of cells surrounding the space in which the search for a solution is required. Several solutions are possible suggesting that the constraint applied to the system of linear equations causes an internal adjustment of the solutions that depends not exclusively from the equations themselves (e.g. boundary values dependency). Beside these conditions that are functions of scale and location, the

computer based method works for all the classes of differential equations considered. Most of the differential equation can be therefore discretised using a finite-difference approach.

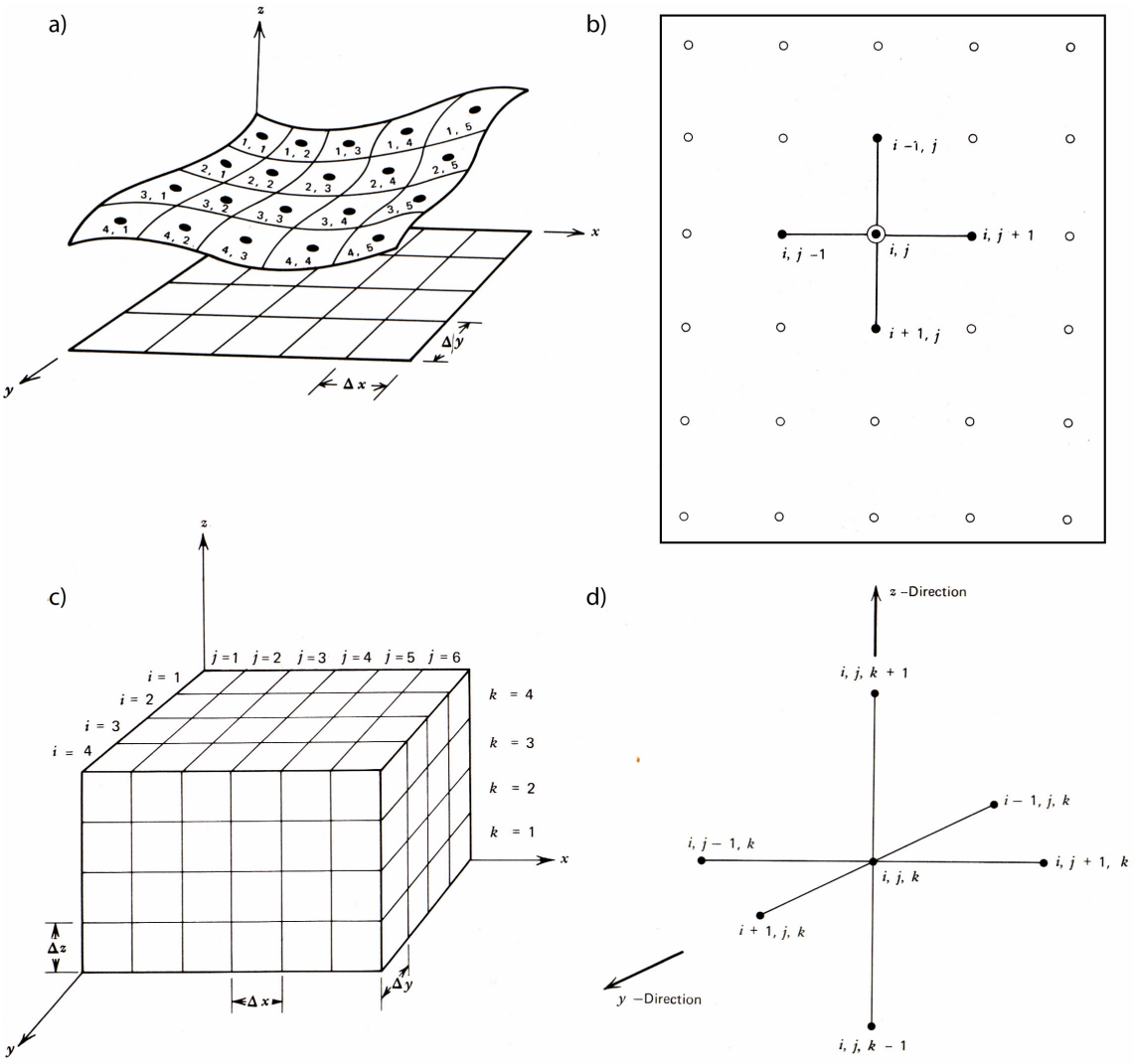

Fig. 2.13 Summary of two- and three-dimensional grids used to discretise the geological continuum. (a) Representation of a continuous function *f*(*x, y*) in *z* with relative indexing used to refer to individual cells defined by intervals $\Delta x, \Delta y$ (b) Four point star method of indexing points implemented for the solution of

partial differential equations of type z = *f*(*x, y*). The star is moved iteratively to adjust the solution from node to node. Usually the partial differential equation is solved alternatively for the variables (*x, y*). (c) Three-dimensional meshwork and relative indexing [*i, j, k*]. (d) Six point star model adopted to solve partial differential equations representing the spatial variation of a generic property Φ as function of (*x, y, z*) coordinates. The finite-difference approximation method is equivalent to the four star model although the star is moved in 3D space. Adapted from Harbaugh and Bonham-Carter (1970).

2.3.3.3 The Lagrangian description

Finite-difference approximations simulating plastic deformation and fluid flow with the aid of a computer represent a reasonable way to handle continuum problems (e.g. using FLAC). This numerical simulation software is composed of different classes of differential equations that deal with specific tasks. For example, FLAC handles the spatial and temporal arrangement of tetrahedrons composing the chosen FLAC-grid during deformation, but also it computes the variation of their spatial organisation as a function of the constitutive relationships and assigned boundary conditions, commonly specified in the numerical model before attempting any kind of simulation. Finite-difference approximation is then used several times to discretise the continuum, both in space and time.

A description of the various classes of equations and their meaning thus follows. In Appendix A the "nodal formulation" is also reviewed for the Newtonian stress/strain relationships considered during deformation of a tetrahedral grid in FLAC (nodal means to reduce the equations to the individual nodes of each tetrahedron composing the FLAC

grid). The equations relative to the Mohr-Coulomb constitutive model and the fluid flow module are also discussed in the end.

2.3.3.3.1 FLAC configuration (explicit finite difference model)

The mathematical background required to understand the following discussion concerns elements of continuum mechanics. For a deeper understanding of some of the concepts presented the reader is referred to Coman (2004). This section outlines how the partial differential equations and mechanical models are organised in the FLAC environment. The structure of the FLAC program is explored looking at the different algorithms.

The Lagrangian dynamic picture of a continuum is the general model adopted in FLAC to describe a body of rock or other materials. The Lagrangian vision is more advanced than classical Newtonian mechanics although preserving the conservation of energy principles. In contrast to Newtonian laws the Lagrangian formulation describes the movement (deformation, fluid flow etc.) of a global system (e.g. a body of fluid or rock) aiming therefore at a generalisation of Newtonian laws to systems composed of multiple particles. (or grid nodes).

2.3.3.3.2 Lagrangian and Eulerian representations (inertial systems)

The Lagrangian description is however not the only formulation available to describe the body motion. The Eulerian description can be also used to account for the spatio/temporal variability of a scalar, vectorial or tensorial field in an even more global manner. This mathematical model differs from the Lagrangian because the same physical laws are constructed upon a different reference system that considers the position of the infinitesimal elements of volume in space. For example, the Lagrangian material description of the body motion (e.g. movement of a rock in space, or a time-dependent flow) is represented at a given position by a particle moving in space and time with velocity $\vec{v}_p(t)$ although no information is given of its position (see Stuart and Tabor, 1990), whereas in the Eulerian space a full description of all the positions of the particles is described $\vec{v}_p\left(\vec{x}\,,\,t\right)$. In other words if a Lagrangian particle moving in space has no certain information of the sort of velocity it will be assuming at a later position (local information only), when computing a partial derivation in time it is also necessary to know its spatial gradient $v_{p\,,p}$. Eulerian particles will assume an expected value represented by the measure of the spatial field, therefore the velocity is already known in space requiring only an ordinary derivation in time $\left(\frac{dv}{dt}\right)$ (see Barr, 2001). Note that the Einstein summation of indexes is used.This is a simple omission of the symbol $\sum$ when

dealing with indexes that sum over one another. For example a vector can be described with three components $\left\{u_1\vec{e}_1, u_2\vec{e}_2, u_3\vec{e}_3\right\}$ such as $\vec{u}=\sum_{i=1}^{3} u_i\, e_i$ that becomes elegantly simplified as $\vec{u}=u_i\,\vec{e_i}$. Note also that in continuum mechanics an index preceded by a comma $\left(\sigma_{ij}\,,_j\right)$ indicates a partial derivation in space of the variable, giving then in more extended form:

$$\sigma_{ij}\,,_j=\frac{\partial\sigma_{i,j}}{\partial x_j} \qquad (2.64).$$

2.3.3.3.3 Cauchy traction tensor and constitutive equations

Equation 2.64 represents the spatial variation of a tensorial field. Here, vectors are distinguished from tensors because a vector is sufficiently represented by three components, whereas six components are necessary to define a tensor. Both objects share an important property which is defined as the *invariance*. An invariant is independent of its reference system. This is a really important point in relativistic theory because the Newtonian Laws are essentially dependent on the considered inertial systems. Relativistic adopting such invariant systems had a more generalized applicability (e.g. Einstein, 1934). Beside the importance in physics the Cauchy's formulae are implemented in

FLAC to define the state of stress and strain of a body. FLAC uses a finite element grid that is composed of tetrahedrons and it will be often necessary to refer to them. Moreover the material points representing the Lagrangian description correspond to the nodes of the tetrahedron subjected to deformation. When a stress is applied to tetrahedrons, these react accumulating stress and rearranging dynamically their shape, thus simulating a state of strain. To characterize this system it is useful then to define a traction vector $\vec{t}$ as follows:

$$t_i = \sigma_{ij} n_j \qquad (2.65).$$

In equation 2.65 the traction is equal to the stress tensor component (σ_{ij}) parallel to the normal (n_j) to each face of the tetrahedron. The distribution of tensions will then control the distribution of stresses in the elements of a whole body. Adding the time dimension leads to deformation as a function of stress- and relative strain-rate. These are quantities representing the ratio between the deformations within a finite interval of time. In particular, the strain-rate in a nodal formulation (Appendix A) can be described by the relative velocities of movement of the nodes of a tetrahedron in FLAC. Two components can be defined for the strain-rate, translational (ξ_{ij}) and rotational (ω_{ij}):

$$\xi_{ij} = \frac{1}{2}\left(v_{i,j} + v_{j,i}\right) \quad (2.66),$$

$$\omega_{ij} = \frac{1}{2}\left(v_{i,j} - v_{j,i}\right) \quad (2.67),$$

with vectorial components of velocity (v_i, v_j) derived respectively in x_j and x_i.

In addition to the basic concepts of stress and strain FLAC also considers two sets of equations in its representation of the plastic deformation: (1) the equations of motion and equilibrium; and (2) the constitutive relationships. The motion of a body is fully described in continuum mechanics with the conservation of momentum relationships (linear, angular and inertial terms of momentum are combined in the Cauchy 's equations of motion). In this regard the formulation in FLAC could be expressed as follows:

$$\sigma_{ij,j} + \rho b_i = \rho \frac{dv_i}{dt} \quad (2.68).$$

Equation 2.68 relates the partial differentiation of the stress tensor (σ_{ij}) to the body force (b_i), which is essentially a field force (e.g. the magnetic and gravitational fields that act indirectly on a body). In contrast, the stress tensor can be considered a contact force. For a unitary mass the action of body and contact forces result in a material derivation in time

of the velocity (an acceleration term). This multiplied by the density (ρ) becomes equivalent to a force. When forces equilibrate the material acceleration is zero.

The equations of motion and the rate of rotational and translational stress and strain can be reduced to a system of 9 linear equations in 15 unknowns therefore requiring the use of six additional equations to solve the deformation of a body. These are the constitutive relationships that are experimental laws for the materials considered in the numerical model (see Appendix A where the Mohr-Coulomb constitutive model is reviewed). The constitutive formulation aims at guessing the state of stress of a certain material in an interval of time in which the material velocities are considered constant inside a tetrahedron. This allows using the rate of strain as a measure of the co-rotational stress-rate tensor $\left[\breve{\sigma}\right]_{ij}$. The constitutive equations can be expressed then in a general form as functions (H) of the stress and strain tensors (σ_{ij}, ξ_{ij}) and also of the loading history considered (k):

$$\left[\breve{\sigma}\right]_{ij} = H_{ij}\left(\sigma_{ij}, \xi_{i,j}, k\right) \tag{2.69}.$$

Such functional relationship represents a constraint for the co-rotational stress-rate tensor that controls the nodal velocities within the model. For a more detailed discussion of the mathematical background behind FLAC refer to Appendix A.

What follows after this introductive section is a series of self-contained chapters intended for individual publications. They are ordered according to the scale of the data sets utilized, from regional scale targeting of mineral deposits through to deposit scale models used to address ore genesis, to even more complex scenarios involving the development of the Lawn Hill Megabreccia.

The flow of the thesis as introduced in Chapter 1 will provide the reader with tangible examples of the different quantitative models discussed. In the end (Chapter 6) this leads to an example of integration of qualitative and quantitative modelling showing that observational science is still important in complex geological problems, in order to obtain an appropriate conceptual model. It is also essential to validate the quantitative analysis.

Most of the thesis focuses on linear techniques to address the geological issues concerning the various studies. A non-linear alternative is also proposed to suggest that more refined mathematical approaches may better describe the deterministic and random components of a system. Chapter 7 proposes an application of these concepts to Pb-Zn mineral systems.